CRYPTIC MICROBES IN ANTARCTICA: DETERMINING THE LIMITS OF BIOTIC DETECTION VIA SATELLITE IMAGERY

Sarah N. Power[1], Mark R. Salvatore[2], and J. E. Barrett[1]

[1]Department of Biological Sciences, Virginia Polytechnic Institute and State University
[2]Department of Astronomy and Planetary Science, Northern Arizona University

Abstract

Autotropic microbial communities are the dominant primary producers in the McMurdo Dry Valleys (MDV) of Antarctica and are therefore the drivers of carbon cycling in this ecosystem. While dense microbial mats occupy aquatic areas in the Taylor Valley, the majority of the landscape is terrestrial where biological surface crusts (*i.e*., biocrusts) occur at much lower densities. Given the broad spatial extent of the terrestrial landscape compared to stream areas, we anticipate most carbon is contained on the soils. While previous research has shown that satellite imagery can be used to detect areas of dense microbial mat and estimate biomass, there are currently no remote sensing methods for systematically estimating biocrust biomass in the dry soils of the MDV. Considering that soils may contain the largest pool of carbon in this region, it is necessary to develop a method that allows for the monitoring of current terrestrial carbon stocks and for predicting future ones. We found that certain geologic minerals drive relatively high NDVI values, creating a false indication of biological activity. While NDVI is proven in detecting dense microbial mat communities, it is now evident that stronger spectral techniques are required to detect low density biocrust communities in this region.

Introduction

Autotropic microbial communities are the drivers of carbon cycling in the McMurdo Dry Valleys (MDV) of Antarctica. These microbial communities consist of cyanobacteria, green algae, diatoms, and moss, are home to microscopic invertebrates, and can form mm – cm thick mats within and nearby aquatic areas and also thin terrestrial crusts on the soil surface. Dense microbial mats commonly inhabit aquatic areas in the Taylor Valley, while the majority of the landscape is terrestrial where biological surface crusts (*i.e*., biocrusts) occupy in much lower densities. The terrestrial landscape is spatially extensive, and although biocrusts on the soils are sparser than the aquatic microbial mats, we anticipate the dry MDV soils contain the most carbon. There are currently no methods for systematically estimating biocrust biomass on the MDV soils over broad spatial scales.

The McMurdo Dry Valleys are the largest contiguous ice-free area on the Antarctic continent, with approximately 4500 km^2 of exposed soil, stream, and lake ecosystems (Levy 2013). Glacial meltwater during the austral summer (*i.e*., 24 hours daylight) forms streams that flow for up to 10 weeks per year (McKnight et al. 1999). These streams feed into perennially ice-covered lakes along the floor of Taylor Valley. While dense microbial mats occupy streams and lake margins (Fig. 1a), biocrusts occupy terrestrial areas in wet depressions, beside snowpacks, and even drier soils (Fig. 1b). The microbial mats and biocrusts are dominated by cyanobacteria (*Nostoc*, *Oscillatoria*, and *Phormidium*) and also contain chlorophyta (green algae), various diatom species (bacillariophyta) (Alger et al. 1997), and

mosses (*Bryum* and *Hennediella*) (Schwarz et al. 1992; Pannewitz et al. 2003).

Fig. 1 Photos of dense microbial mat beside stream (**a**) and sparse biocrust in terrestrial area nearby snowpack (**b**).

In addition, simple metazoan communities of nematodes, rotifers, and tardigrades inhabit the soils and sediments of this region (Freckman and Virginia 1997). Nematodes (*i.e.*, microscopic roundworms that consume cyanobacteria and other microbes) are the most widely distributed metazoan taxa in this region (Freckman and Virginia 1997). Though, given such low soil biomass, negligible grazing influences on microbial mat communities (Treonis et al. 1999) makes the MDV a simple system for studying biocrust.

Taylor Valley is composed of tills (*i.e.*, unsorted soil/rock material deposited directly from glacial ice) from different sequences of glaciations. Most notably, the Ross till (Fig. 2), deposited directly from Ross Sea ice sheets in the late Pleistocene (Bockheim et al. 2008), is on the eastern side of Taylor Valley and is considered the most productive area of this valley, as it is closest to the coast, is relatively humid, has relatively high soil moisture content compared to the other climate zones in this region (Marchant and Denton 1996; Doran et al. 2002), and has the most active and fully functioning soil communities (Adams et al. 2006; Barrett et al. 2006b). While soil environments outside of stream channels do not commonly support visible microbial mat biomass, they are, however, spatially extensive compared to the wetted areas. Due to the broad spatial extent of these terrestrial environments, even sparse spatial distributions of biocrusts could sum to more biomass overall. The question posed here is a fundamental one relevant for carbon budgets and predicting future carbon stocks and is useful for understanding the basic ecology of this ecosystem. To quantify the relative proportion of biomass in the terrestrial areas of the Ross till, a new scalable method is required.

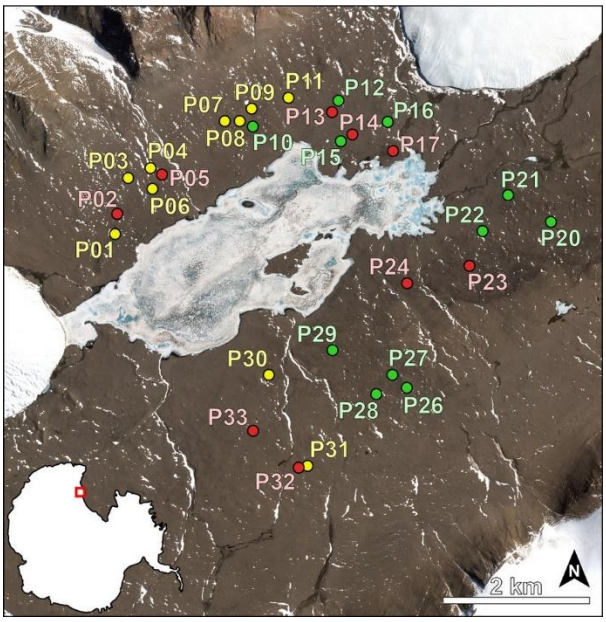

Fig. 2 True color image of Ross till region with the 30 sampling locations identified with varying NDVI values (green refers to "high" NDVI, yellow "variable", and red "low"). Inset in bottom left corner shows Antarctica with red box outlining the McMurdo Dry Valleys. Imagery © 2018 DigitalGlobe, Inc.

We have shown the utility of multispectral satellites WorldView-2 and

WorldView-3 (WV-2/3) in detecting microbial mats in densely colonized areas near streams on the Ross till using the normalized difference vegetation index (NDVI) (Salvatore 2015; Salvatore et al. 2020; Power et al. 2020). NDVI evaluates the relationship between reflectance at 680 and 800 nm where photosynthetic materials exhibit a strong diagnostic signal. This signal is caused by vegetation, which has a unique spectral signature of absorbance in the visible wavelengths (due to the activity of chlorophyll-a and other pigments) and strong reflectance in near-infrared regions due to scattering and reflectance by cell walls. Additionally, we have observed NDVI values indicative of photosynthetic activity in upland areas not connected to streams or lakes (Power et al. 2020). While NDVI is a useful indicator of biological activity in dense areas, it is unknown whether these anomalously high NDVI values in non-wetland areas support photosynthetic activity or are simply background noise of the satellite image associated with some other topographical or geological attribute.

These drier soil environments have received significant attention and have been shown to support fully functioning and active food webs, even given the low diversity of taxa in soils (Freckman and Virginia 1997; Courtright et al. 2001; Barrett et al. 2006a; Barrett et al. 2006b; Poage et al. 2008). The MDV soil community consists of cyanobacteria (and other prokaryotes), algae (*e.g.*, diatoms), mosses, lichens, nematodes, tardigrades, rotifers, fungi, protozoans (*i.e.*, flagellates, amoebae, ciliates), and microarthropods (*i.e.*, springtails and mites) (Adams et al. 2006). Because these soils host active microbial and invertebrate communities and have detectable surface chlorophyll-a content (*e.g.*, Barrett et al. 2004), we predict these "NDVI anomalies" are suggestive of photosynthetic life supporting active food webs. While the wetter soils (*e.g.*, stream and lake margins) receive more attention, we think the drier soils may be equally important, if not more, to the overall carbon budget of the McMurdo Dry Valleys.

We proposed to answer the following question:

Q1: Can WorldView-2 satellite imagery detect cryptic biological activity in Antarctic soils (*i.e.*, are low, but detectable, readings of NDVI indicative of biological activity)?

Combining multispectral satellite imagery, handheld hyperspectral data, and biological ground truthing data, we test the ability for WorldView-2 satellite to detect cryptic patches of biological activity in the form of biocrusts in terrestrial soils of the McMurdo Dry Valleys.

Methods

Field collection

Using December 2018 WV-2 imagery, we identified 30 locations on the Ross till with varying NDVI values. These terrestrial sites consist of drier soils unconnected by stream or lake margins (*i.e.*, referred to as "upland areas"). This imagery was overlain with a digital elevation model (DEM) of 1 m resolution (Fountain et al. 2017) to identify sites in depressions, rocky outcrops, and on slopes and hills. In late December 2019, we located and sampled these 30 varying NDVI sites. We obtained photographs and noted the field conditions (*e.g.*, dry soils with no indication of biological activity, wet soils with snowpack nearby, area dominated by specific geology, *etc.*). We collected a top layer of soil and rock from all sites for subsequent hyperspectral analysis. At 12 of the sites, we established 5 m x 5 m plots (Fig. 3) and collected 5 top layer soil samples (one from each corner and center) of a known area (128 cm^2) for pigment analysis (chlorophyll-a, scytonemin, and carotenoids) and ash-free dry mass (AFDM) for organic matter content. We also collected underlying soil (top 10 cm) for

moisture content, conductivity, pH, inorganic nitrogen concentration in the form of ammonium (NH_4^+) and nitrate (NO_3^-), and invertebrate abundance (nematodes, tardigrades, rotifers).

Fig. 3 Photo of Plot 01, wet depression, showing plot area outlined by 5 x 5 m transect.

Laboratory analyses

Using the top layer soil samples, we determined pigment concentration using a trichromatic spectrophotometric method for chlorophyll-a, carotenoids, and scytonemin at 663, 490, and 384 nm, respectively (Garcia-Pichel and Castenholz 1991). Throughout the process, care was taken to avoid exposing the samples to light, as chlorophyll-a degrades with light exposure. The samples were first dried at 105°C for 24 hr, sieved through a 4 mm sieve, and extracted for 24 hr at ambient temperature in 90% unbuffered acetone using a 3.75:10 soil to solvent ratio, based on protocols from Couradeau et al. (2016) and MCM LTER standard methods. After centrifugation, the extracts were analyzed on a spectrophotometer using 10 mL cuvettes. The absorbances contributed by each pigment were calculated using the trichromatic equations outlined in Garcia-Pichel and Castenholz (1991), and the pigment concentrations were calculated using the Beer-Lambert Law with the extinction coefficients of 89.7 L g^{-1} cm^{-1} for chlorophyll-a (Couradeau et al. 2016), 112.6 L g^{-1} cm^{-1} for scytonemin (Brenowitz and Castenholz 1997), and 262 L g^{-1} cm^{-1} for carotenoids (Thrane et al. 2015). Additionally, the top layer soil samples were measured for AFDM by weighing a known area of sample, combusting at 550°C for 24 hr using a muffle furnace, gently stirring samples halfway through combustion, and reweighing after cooling in a desiccator. Given the extremely low clay content of soils in this region (Barrett et al. 2006a), the rehydration of clays was assumed negligible, so we did not rewet samples.

From the underlying soil samples, we measured percent moisture content, and pH and electrical conductivity using a 1:2 and 1:5 soil to DI H_2O slurry, respectively. We also extracted inorganic N in the form of NH_4^+ and NO_3^- with a 2:5 soil to KCL extract using a Lachat flow injection analyzer. Invertebrate abundance was enumerated on the underlying soil using a modified sugar-centrifugation method (Freckman and Virginia 1993).

Spectral collection and analysis

WorldView-2 (DigitalGlobe, Inc.) is an 8-band multispectral satellite on polar orbit with 1.84 m resolution at nadir. Images acquired between December 2018 and December 2019 were used to identify varying NDVI upland terrestrial areas and correlate them to biological ground truthing data, respectively. The imagery was georeferenced using ground control points and then obtained from the University of Minnesota's Polar Geospatial Center (PGC) through a cooperative agreement between the NSF and National Geospatial-Intelligence Agency (NGA). Data were subsequently processed to atmospherically corrected surface reflectance using five spectral ground validation targets acquired in the field during the 2018-2019 austral summer (Salvatore et al. *in review*). Band-specific linear relationships between top-of-atmosphere reflectance data and ground

validation spectra were applied to the entirety of the satellite images to remove atmospheric contributions to the observed signal. The NDVI parameter was calculated using the Environment for Visualizing Images (ENVI, Harris Geospatial) software package. NDVI is a common vegetation index used for determining whether an image contains photosynthesizing vegetation (Tucker 1979). NDVI was calculated as:

$$NDVI = \frac{\rho_{NIR} - \rho_{Red}}{\rho_{NIR} + \rho_{Red}}$$

where ρ_{NIR} and ρ_{Red} represent the spectral reflectance measurements acquired in the near-infrared (WorldView-2 Band 7, centered at 831 nm) and red (WorldView-2 Band 5, centered at 659 nm) regions, respectively. The varying NDVI locations were identified as occurring within depressions, on slopes or hills, and within rocky outcrops by using a (DEM) of 1 m resolution (Fountain et al. 2017). NDVI was extracted from the 4 pixels centered at each plot location, based on GPS coordinates taken during sampling and visually confirming plot location via nearby boulders, snowpacks, etc. The primary WorldView-2 image used in this analysis (103001009FA0AE00) was acquired on December 3, 2019, approximately three weeks before our field sampling campaign. Map products were created using ArcMap (ESRI).

Hyperspectral reflectance data were acquired for top layer soil samples collected in the field. These data were acquired using an Analytical Spectral Devices (ASD) FieldSpec4 high-resolution hyperspectral reflectance spectrometer, set up for use in a stable lab environment. Data were collected between 350 and 2500 nm with 1 nm sampling. Halogen lamps were used to illuminate the samples at 30° off-nadir, while reflectance was measured using the ASD's fiber optic cable at nadir. Measurements represent an average of 50 individual spectra, which were averaged to minimize noise and to ensure a representative spectral signature. Soil samples were shipped frozen from Virginia Tech to Northern Arizona University where the spectral measurements were acquired.

Statistical analysis

Statistical analyses were performed using R Statistical Software version 4.0.3 (R Core Team). Principal components analyses (PCA) were executed using R to visually compare plots and their NDVI in terms of their soil habitat environment and biological activity. We also performed correlation analyses using the average NDVI plot values with the biological parameters (*i.e.*, pigments, AFDM) averaged for each of the plots as well. Each point on the scatter plot represents one plot location, resulting in 7 observations. Linear regressions of means were fit in R.

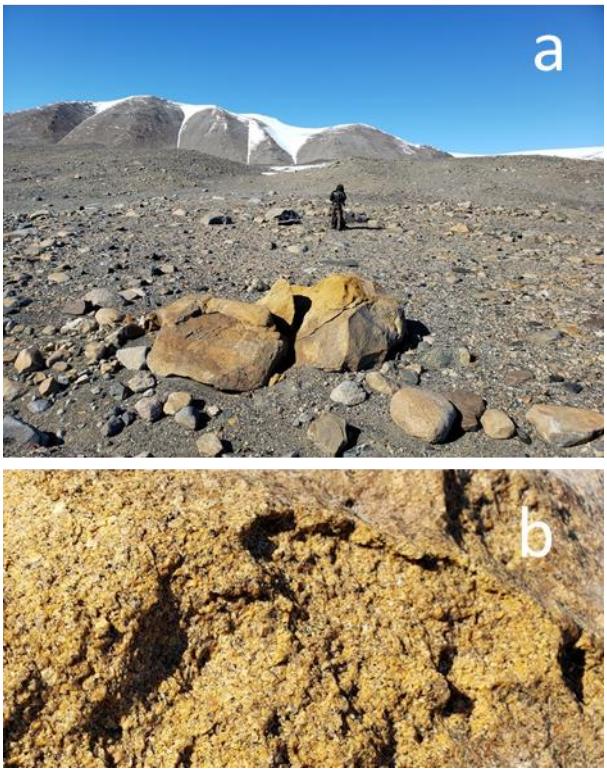

Fig. 4 Photos of relatively high NDVI Plot 20 oxidized granite (**a**) and close-up granite view (**b**).

Results

After locating the varying NDVI sites in the field, we determined that many of the locations seemed visually plausible for suitable habitats (*i.e.*, wet soils, depressions, snowpacks nearby, *etc.*). One location in particular had dense biocrust present (Plot 09), while other plots were identified as possibly containing sparse biocrust cover (*e.g.*, Plot 04, Plot 11). Alternatively, there were several plot locations that were categorized as having relatively high NDVI that, upon examination, were dry, barren, and seemingly uninhabitable. Many of these relatively high NDVI locations, however, were scattered with bright orange rocks visually identified as oxidized granite (Fig. 4). While many of these relatively high NDVI locations seemed indicative of true biological activity, there were clearly some locations where geology was driving NDVI rather than biology.

Table 1. Average values for the 12 intensively sampled plots ± 1 standard deviation. NDVI data shown were extracted from WV-2 December 2019 imagery.

Plot	NDVI	AFDM (mg cm^{-2})	Chlorophyll (µg cm^{-2})	Moisture content (%)	Conductivity (µS cm^{-1})	pH	mg NO_3^- g^{-1} soil
P01	-0.008 ± 0.000	5.35 ± 2.51	0.009 ± 0.006	5.39 ± 2.69	2330 ± 2073	8.4 ± 1.14	23.15 ± 21.8
P09	-0.008 ± 0.005	28.29 ± 19.34	4.974 ± 5.097	5.77 ± 3.13	70 ± 33	8.5 ± 0.60	0.34 ± 0.13
P10	0.009 ± 0.005	2.12 ± 0.44	0.007 ± 0.002	1.54 ± 0.29	112 ± 44	9.9 ± 0.32	0.001 ± 0.002
P14	-0.007 ± 0.005	4.06 ± 0.95	0.006 ± 0.006	5.81 ± 1.79	2311 ± 1627	8.6 ± 0.66	19.32 ± 15.7
P17	-0.017 ± 0.003	3.90 ± 0.70	0.005 ± 0.003	2.34 ± 0.63	1095 ± 585	8.8 ± 0.48	26.32 ± 25.5
P22	0.001 ± 0.007	2.19 ± 0.85	0.005 ± 0.002	4.92 ± 1.29	2152 ± 703	9.5 ± 0.51	26.20 ± 18.3
P23	-0.022 ± 0.003	2.99 ± 0.77	0.002 ± 0.002	2.23 ± 1.15	907 ± 253	9.6 ± 0.55	5.37 ± 2.52
P27	0.008 ± 0.004	3.18 ± 1.00	0.006 ± 0.003	3.18 ± 3.50	656 ± 468	8.4 ± 0.25	1.73 ± 2.13
P28	-0.008 ± 0.003	2.55 ± 0.46	0.003 ± 0.002	6.56 ± 6.47	515 ± 394	8.9 ± 0.43	2.07 ± 2.51
P30	-0.014 ± 0.004	3.46 ± 0.51	0.005 ± 0.003	4.02 ± 2.63	2347 ± 2328	9.0 ± 0.74	13.36 ± 16.5
P31	-0.023 ± 0.001	3.87 ± 0.69	0.007 ± 0.002	4.61 ± 1.41	2431 ± 1572	8.2 ± 0.22	11.07 ± 8.0
P33	-0.015 ± 0.003	2.61 ± 0.75	0.004 ± 0.002	2.30 ± 0.24	130 ± 60	9.6 ± 0.24	0.05 ± 0.10

There was significant variation among the sites in terms of soil variables (moisture content, pH, conductivity, NH_4^+ and NO_3^- concentration) and biological variables (concentration of chlorophyll-a, carotenoids, scytonemin, AFDM, and population of invertebrates) (Table 1). Notably, Plot 09 with visible biocrust had the highest diversity consisting of all three nematode species (*Scottnema*, *Eudorylaimus*, and *Plectus*), tardigrades, rotifers, and even ciliates. While *Scottnema* was present in relatively high abundances throughout the plots, there were several plots without any invertebrates present (P22, 30, 31). The majority of samples had NH_4^+ concentration below detection, except for Plots 01, 09, 10, 22, 31, 33, which were detectable, though very low concentrations.

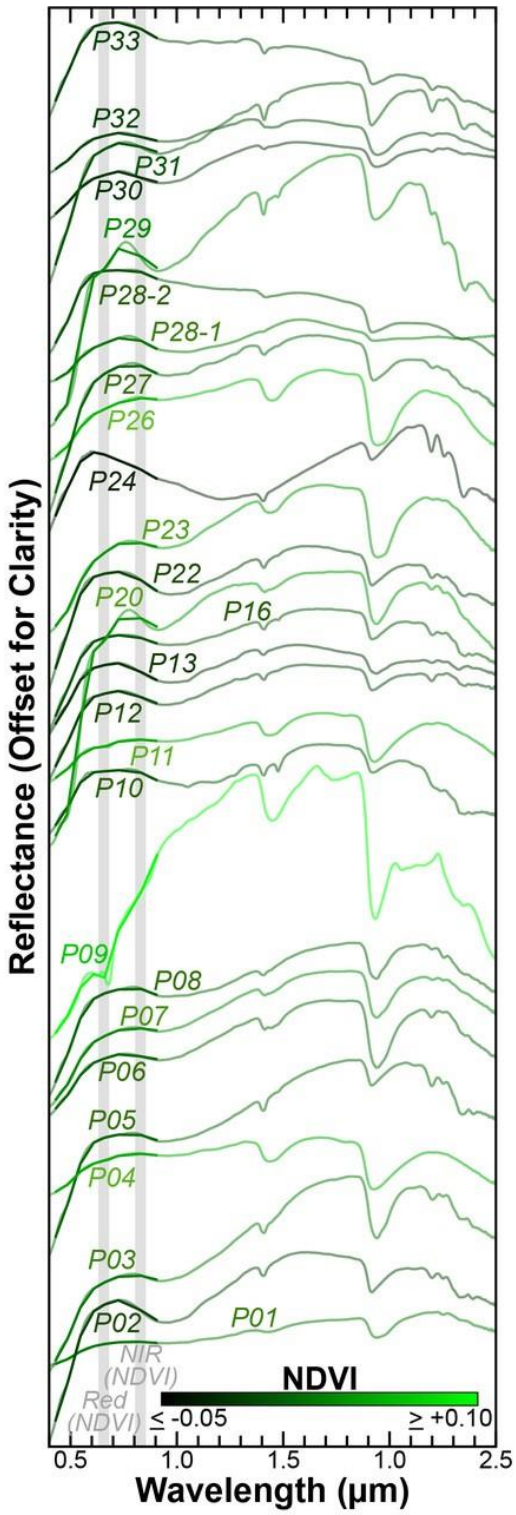

Fig. 5 Spectra acquired from samples using a hyperspectral imaging spectrometer. Spectra downsampled to WV-2 resolution are shown in bold in the NDVI identified region of the spectrum.

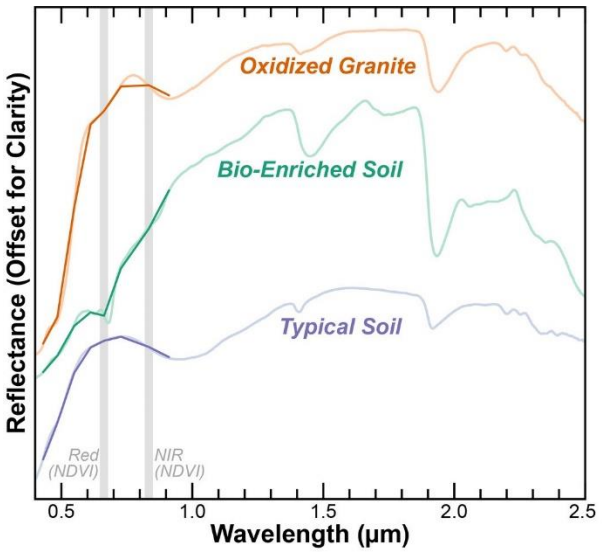

Fig. 6 Three spectral signatures illustrating relatively high NDVI from biocrust (Plot 09) and oxidized granite (Plot 20) and relatively low NDVI from typical soil (Plot 02). Spectra downsampled to WV-2 resolution are shown in bold. Gray bars outline the region of NDVI calculation.

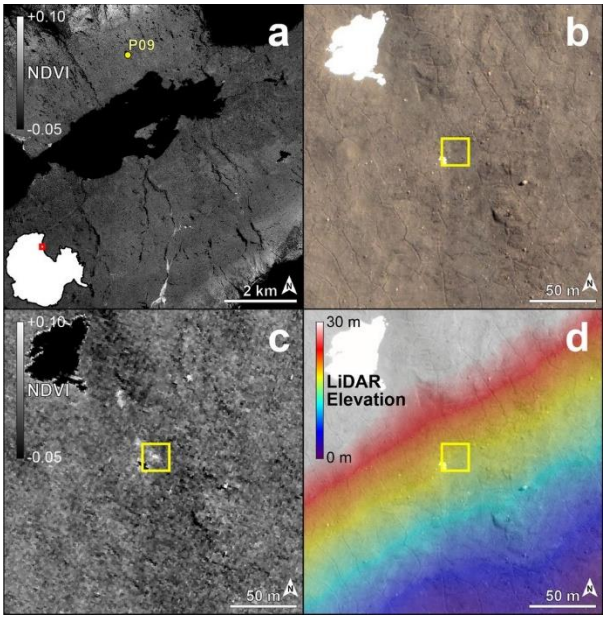

Fig. 7 a.) NDVI product of Ross till region with Plot 09 identified, **b.)** True color image of Plot 09 and surrounding area **c.)** NDVI product and **d.)** LiDAR elevation with Plot 09 outlined in yellow. Imagery © 2019 DigitalGlobe, Inc.

Hyperspectral data of samples collected show variation among the 30 plot locations (Fig. 5). There is a range in NDVI between the sites, and in particular, there are clear spectral differences between the plots, for example, Plots 09 (biocrust) and 20 (oxidized granite). While they both have relatively high NDVI, it is evident that the shape of their spectral signatures is very different. These differences are further illustrated in Fig. 6, which compares the spectral shape of relatively high NDVI Plots 09 and 20 with a barren soil Plot 02.

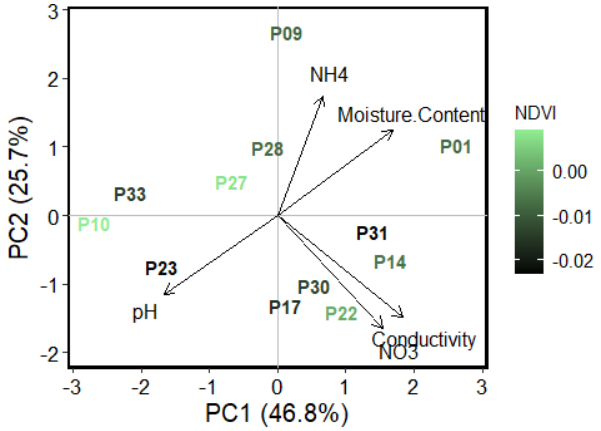

Fig. 8 PCA with soil habitat vectors illustrating increasing values. NDVI based on satellite-derived plot average.

Using the WV-2 satellite imagery, we identified the plot locations as unique compared to the surrounding areas based on NDVI. The densest biocrust plot is visually identifiable using NDVI (Fig. 7). Using principal components analysis (PCA) with the soil habitat variables, the plots separate in ordination space based on moisture content, pH, conductivity, and inorganic nitrogen content (Fig 8). There is not an obvious separation between the relatively high NDVI and low NDVI plots. Similarly, in a PCA with the biological variables, the plots separate in ordination space based on chlorophyll content, AFDM, and total live nematode counts (Fig. 9). Figure 9 does not include Plot 09, because its far-right distribution in ordination space (due to significantly higher biomass and chlorophyll content) clustered the rest of the plots into an uninterpretable ordination space.

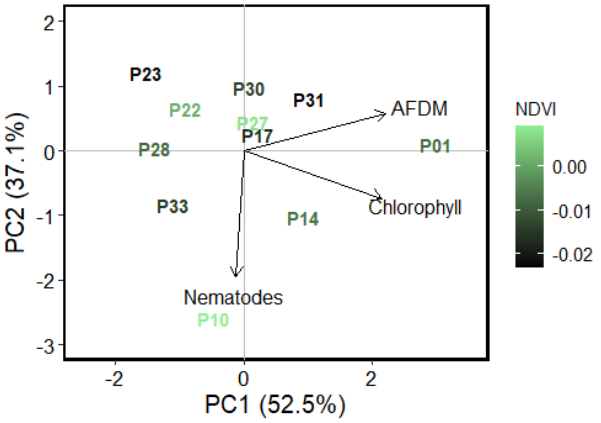

Fig. 9 PCA with biological vectors illustrating increasing values. NDVI based on satellite-derived plot average.

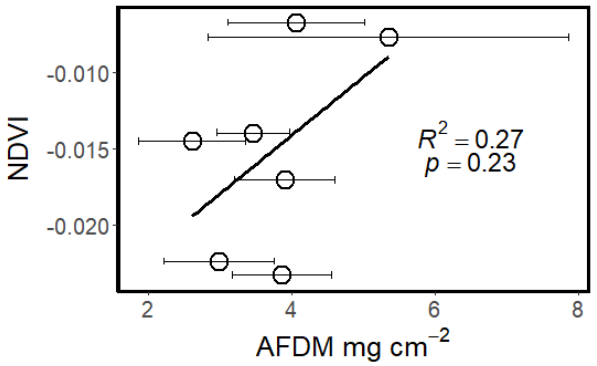

Fig. 10 Non-significant linear relationship between AFDM and NDVI. Error bars indicate population standard deviation. Plots 09 and 10, 22, 27, 28 not shown.

When correlating the satellite-derived NDVI plot averages to the measured biological variables, no relationships were significant. When including all plots in the analysis, Plot 09 skewed the scatter plots due to its much higher AFDM and pigment concentration, so this plot was excluded. Additionally, since we are now aware that several plots had high NDVI associated with oxidized granite, these plots were also removed from the correlation analyses (P10, 22, 27, 28). Out of the 12 intensively sampled plots, these were determined to have a high cover of oxidized

granite based on field photos, field notes, and hyperspectral signatures. Even with these plots removed, the correlation analyses were still non-significant ($p > 0.05$) (Fig 10, 11).

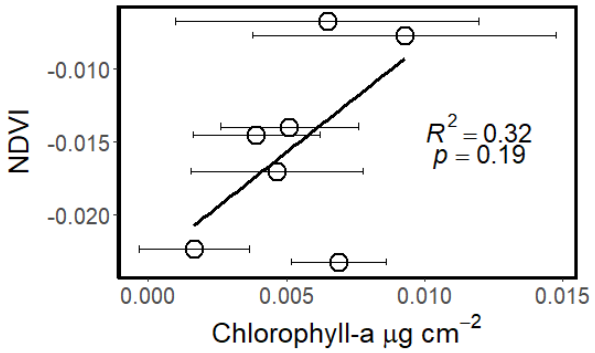

Fig. 11 Non-significant linear relationship between chlorophyll-a concentration and NDVI. Error bars indicate population standard deviation. Plots 09 and 10, 22, 27, 28 not shown.

Discussion

It was evident during ground truthing that geology would be a factor in confirming the utility of NDVI for detection of low biomass biocrusts in this region. Several plots that we had identified as relatively high NDVI sites were visually dry and covered with oxidized granite and proved to have relatively low AFDM and chlorophyll content. Following along with this pattern, the hyperspectral data later collected from field samples showed clear distinctions between the plots. For example, Plots 20 and 29 were on oxidized granite boulder fields (according to field notes and photos) and exhibit two broad electronic absorptions associated with the presence of ferrous and ferric iron, centered near 670 nm and 940 nm, and resulting in a broad reflectance peak between these two absorptions at approximately 740 nm (Fig 6.). Hyperspectral reflectance data are able to clearly distinguish between these abiotic absorption features and those associated with biological pigments; however, multispectral data are less helpful in making this distinction. For this reason, we have shown that the NDVI parameter specifically can be problematic at identifying the presence of photosynthetic biology in the presence of specific abiotic surface properties. This electronic Fe-absorption at red wavelengths and the slight increase in reflectance in the NIR causes these granite areas to have an anomalously high NDVI that does not appear to be correlated with any biological activity. It is noteworthy that Plot 09, the only plot with visibly dense biocrust, is visually unique with the highest NDVI in the hyperspectral data (Fig. 5), however it does not have the highest satellite-derived NDVI (Table 1). This clearly shows the differences in resolution and capability between a hyperspectral imaging spectrometer and a multispectral satellite. Additionally, this difference could also partly be the result of activity, as a January 2019 image shows higher NDVI at this location when the snow is melting. While Plot 09 was expected to have been the highest satellite-derived NDVI site, this was not the case, so it is apparent there are factors here, other than biomass, driving NDVI.

The principal component analyses also indicate that biological activity is not the only factor driving NDVI in this region. While we would expect the higher NDVI plots to cluster in the top right corner of the ordination with increasing NH_4^+ and moisture content, there was no clear pattern with NDVI (Fig. 8). Specifically, it is of interest that Plots 10, 22, and 27 had the highest satellite-derived NDVI but do not cluster in the top right quadrant of the ordination space. Similarly, there are no obvious patterns of clustering by NDVI when visualizing the biological variables (Fig. 9). We would expect the highest NDVI plots to cluster in the far right of the ordination space, but these oxidized granite plots are seemingly not biologically active. Therefore, we chose to remove Plots 09 and 10, 22, 27, and 28 from the correlation analyses because the highest biomass plot skews the analysis and the oxidized granite creates a false indication of

biological activity, respectively. We found that there was no significant relationship between NDVI and the biological variables. However, we are not surprised. The Ross till region is geologically variable, and it is now evident that certain geological minerals can have a relatively high NDVI, adding unexpected complexity to our objective of detecting cryptic biological activity.

We will apply different indices and image analysis techniques to better establish the spectral capabilities of detecting such low density biocrust coverage. While it is evident that NDVI is a useful indicator of dense microbial mat cover in the McMurdo Dry Valleys, we now require more in-depth spectral analyses for low density biocrust areas. We are confident that different techniques using all 8 spectral bands we have available with WorldView-2 will allow us to systematically identify the abundance and distribution of low density biocrust throughout the Ross till terrestrial region.

Acknowledgments

This project was supported by the Virginia Space Grant Consortium 2020 Fellowship Program and the National Science Foundation through Grant #1637708 to the McMurdo Dry Valleys Long Term Ecological Research Project and Grant #1745053 to Salvatore, Barrett, Sokol, and Stanish. We acknowledge the Polar Geospatial Center for geospatial support and DigitalGlobe, Inc. for access to satellite imagery. We appreciate Antarctic Support Contractors and Air Center Helicopters for providing operational support in the field. We'd also like to thank Ernest Osburn for assistance with sample collection in the field, and Bobbie Niederlehner, Byron Adams, and Maxwell Craddock for their assistance with laboratory analyses.

References

Adams BJ, Bardgett RD, Ayres E, Wall DH, Aislabie J, Bamforth S, Bargagli R, Cary C, Cavacini P, Connell L, Convey P, Fell JW, Frati F, Hogg ID, Newsham KK, O'Donnell A, Russell N, Seppelt RD, Stevens MI (2006) Diversity and distribution of Victoria Land biota. Soil Biol Biochem 38:3003–3018 . https://doi.org/10.1016/J.SOILBIO.2006.04.030

Alger AS, McKnight DM, Spalding SA, Tate CM, Shupe GH, Welch KA, Edwards R, Andrews ED, House HR (1997) Ecological Processes in a Cold Desert Ecosystem: The Abundance and Species Distribution of Algal Mats in Glacial Meltwater Streams in Taylor Valley, Antarctica. Inst Arct Alp Res Occas Pap 51

Barrett JE, Virginia RA, Hopkins DW, Aislabie J, Bargagli R, Bockheim JG, Campbell IB, Lyons WB, Moorhead DL, Nkem JN, Sletten RS, Steltzer H, Wall DH, Wallenstein MD (2006a) Terrestrial ecosystem processes of Victoria Land, Antarctica. Soil Biol Biochem 38:3019–3034 . https://doi.org/10.1016/J.SOILBIO.2006.04.041

Barrett JE, Virginia RA, Wall DH, Cary SC, Adams BJ, Hacker AL, Aislabie JM (2006b) Co-variation in soil biodiversity and biogeochemistry in northern and southern Victoria Land, Antarctica. Antarct Sci 18:535 . https://doi.org/10.1017/S0954102006000587

Barrett JE, Virginia RA, Wall DH, Parsons AN, Burkins MB (2004) Variation in Biogeochemistry and Soil Biodiversity across Spatial Scales in a Polar Desert Ecosystem. Ecology 85:3105–3118

Bockheim JG, Prentice ML, McLeod M (2008) Distribution of glacial deposits, soils, and permafrost in Taylor Valley, Antarctica. Arctic, Antarct Alp Res 40:279–286 . https://doi.org/10.1657/1523-0430(06-057)[BOCKHEIM]2.0.CO;2

Brenowitz S, Castenholz RW (1997) Long-term effects of UV and visible irradiance on natural populations of a scytonemin-containing cyanobacterium (Calothrix sp.). FEMS Microbiol Ecol 24:343–352 . https://doi.org/10.1016/S0168-6496(97)00075-5

Couradeau E, Karaoz U, Lim HC, Nunes Da Rocha U, Northen T, Brodie E, Garcia-Pichel F (2016) Bacteria increase arid-land soil surface temperature through the production of sunscreens. Nat Commun. https://doi.org/10.1038/ncomms10373

Courtright EM, Wall DH, Virginia RA (2001) Determining habitat suitability for soil invertebrates in an extreme environment: The McMurdo Dry Valleys, Antarctica. Antarct Sci

13:9–17 . https://doi.org/10.1017/S0954102001000037
Doran PT, McKay CP, Clow GD, Dana GL, Fountain AG, Nylen T, Lyons WB (2002) Valley floor climate observations from the McMurdo dry valleys, Antarctica, 1986–2000. J Geophys Res 107:4772 . https://doi.org/10.1029/2001JD002045
Fountain AG, Fernandez-Diaz JC, Obryk M, Levy J, Gooseff M, Van Horn DJ, Morin P, Shrestha R (2017) High-resolution elevation mapping of the McMurdo Dry Valleys, Antarctica, and surrounding regions. Earth Syst Sci Data 9:435–443 . https://doi.org/10.5194/essd-9-435-2017
Freckman DW, Virginia RA (1997) Low-diversity antarctic soil nematode communities: Distribution and response to disturbance. Ecology 78:363–369 . https://doi.org/10.1890/0012-9658(1997)078[0363:LDASNC]2.0.CO;2
Freckman DW, Virginia RA (1993) Extraction of nematodes from Dry Valley Antarctic soils. Polar Biol 13:483–487 . https://doi.org/10.1007/BF00233139
Garcia-Pichel F, Castenholz RW (1991) Characterization and Biological Implications of Scytonemin, a Cyanobacterial Sheath Pigment. J Phycol 27:395–409 . https://doi.org/10.1111/j.0022-3646.1991.00395.x
Levy J (2013) How big are the McMurdo Dry Valleys? Estimating ice-free area using Landsat image data. Antarct Sci 25:119–120 . https://doi.org/10.1017/S0954102012000727
Marchant DR, Denton GH (1996) Miocene and Pliocene paleoclimate of the Dry Valleys region, Southern Victoria land: A geomorphological approach. Mar Micropaleontol 27:253–271 . https://doi.org/10.1016/0377-8398(95)00065-8
McKnight DM, Niyogi DK, Alger AS, Bomblies A, Conovitz PA, Tate CM (1999) Dry Valley Streams in Antarctica: Ecosystems Waiting for Water. Bioscience 49:985–995 . https://doi.org/10.1525/bisi.1999.49.12.985
Pannewitz S, Green TGA, Scheidegger C, Schlensog M, Schroeter B (2003) Activity pattern of the moss Hennediella heimii (Hedw.) Zand. in the Dry Valleys, Southern Victoria Land, Antarctica during the mid-austral summer. Polar Biol 26:545–551 . https://doi.org/10.1007/s00300-003-0518-8
Poage MA, Barrett JE, Virginia RA, Wall DH (2008) The influence of soil geochemistry on nematode distribution, Mcmurdo Dry Valleys, Antarctica. Arctic, Antarct Alp Res 40:119–128 . https://doi.org/10.1657/1523-0430(06-051)[POAGE]2.0.CO;2
Power SN, Salvatore MR, Sokol ER, Stanish LF, Barrett JE (2020) Estimating microbial mat biomass in the McMurdo Dry Valleys, Antarctica using satellite imagery and ground surveys. Polar Biol 1–15 . https://doi.org/10.1007/s00300-020-02742-y
Salvatore MR (2015) High-resolution compositional remote sensing of the Transantarctic Mountains: application to the WorldView-2 dataset. Antarct Sci 27:473–491 . https://doi.org/10.1017/S095410201500019X
Salvatore, MR., Borges SR, Barrett JE, Power SN, Stanish LF, and Sokol ER. *In review.* Counting Carbon: Quantifying Biomass in the McMurdo Dry Valleys through Orbital & Field Observations.
Salvatore MR, Borges SR, Barrett JE, Sokol ER, Stanish LF, Power SN, Morin P (2020) Remote characterization of photosynthetic communities in the Fryxell basin of Taylor Valley, Antarctica. Antarct Sci 1–16 . https://doi.org/10.1017/S0954102020000176
Salvatore MR, Mustard JF, Head JW, Marchant DR, Wyatt MB (2014) Characterization of spectral and geochemical variability within the Ferrar Dolerite of the McMurdo Dry Valleys, Antarctica: weathering, alteration, and magmatic processes. Antarct Sci 26:49–68 . https://doi.org/10.1017/S0954102013000254
Schwarz AMJ, Green TGA, Seppelt RD (1992) Terrestrial vegetation at Canada Glacier, Southern Victoria Land, Antarctica. Polar Biol 12:397–404 . https://doi.org/10.1007/BF00243110
Thrane J-E, Kyle M, Striebel M, Haande S, Grung M, Rohrlack T, Andersen T (2015) Spectrophotometric Analysis of Pigments: A Critical Assessment of a High-Throughput Method for Analysis of Algal Pigment Mixtures by Spectral Deconvolution. PLoS One 10:e0137645 . https://doi.org/10.1371/journal.pone.0137645
Treonis A, Wall D, Virginia R (1999) Invertebrate biodiversity in Antarctic Dry Valley soils and sediments. Ecosystems 2:482–492
Tucker CJ (1979) Red and Photographic Infrared Linear Combinations for Monitoring Vegetation. Remote Sens Environ 8:127–150